Aging-associated REGγ proteasome decline predisposes to tauopathy

Received for publication, June 27, 2022, and in revised form, September 20, 2022 Published, Papers in Press, October 7, 2022,
https://doi.org/10.1016/j.jbc.2022.102571

Jialu Tu[1,‡], Haiyang Zhang[1,‡], Ting Yang[1], Yun Liu[1], Solomon Kibreab[1], Yunpeng Zhang[1], Liangcai Gao[1], Robb E. Moses[2], Bert W. O'Malley[2], Jianru Xiao[3,*], and Xiaotao Li[2,4,5,*]

From the [1]Institute of Biomedical Sciences, Shanghai Key Laboratory of Brain Functional Genomics (Ministry of Education), School of Life Sciences, East China Normal University, Shanghai, China; [2]Department of Molecular and Cellular Biology, Dan L. Duncan Cancer Center, Baylor College of Medicine, Houston, Texas, USA; [3]Department of Orthopedic Oncology, Changzheng Hospital, The Second Military Medical University, Shanghai, China; [4]School of Arts and Sciences, New York University-Shanghai, Shanghai, China; [5]Key Laboratory of Epigenetics and Oncology, the Research Center for Preclinical Medicine, Southwest Medical University, Luzhou, Sichuan, China

Edited by Elizabeth Coulson

The REGγ-20S proteasome is an ubiquitin- and ATP-independent degradation system, targeting selective substrates, possibly helping to regulate aging. The studies we report here demonstrate that aging-associated REGγ decline predisposes to decreasing tau turnover, as in a tauopathy. The REGγ proteasome promotes degradation of human and mouse tau, notably phosphorylated tau and toxic tau oligomers that shuttle between the cytoplasm and nuclei. REGγ-mediated proteasomal degradation of tau was validated in 3- to 12-month-old *REGγ* KO mice, *REGγ* KO;PS19 mice, and PS19 mice with forebrain conditional neuron-specific overexpression of REGγ (*REGγ* OE) and behavioral abnormalities. Coupled with tau accumulation, we found with REGγ-deficiency, neuron loss, dendrite reduction, tau filament accumulation, and microglial activation are much more prominent in the *REGγ* KO;PS19 than the PS19 model. Moreover, we observed that the degenerative neuronal lesions and aberrant behaviors were alleviated in *REGγ* OE;PS19 mice. Memory and other behavior analysis substantiate the role of REGγ in prevention of tauopathy-like symptoms. In addition, we investigated the potential mechanism underlying aging-related REGγ decline. This study provides valuable insights into the novel regulatory mechanisms and potential therapeutic targets for tau-related neurodegenerative diseases.

Aberrant accumulation of filamentous tau lesions, which are a characteristic feature of Alzheimer's disease (AD) and tauopathies, is the most common neuropathological manifestation in several neurodegenerative diseases, such as progressive supranuclear palsy, Pick's disease, frontotemporal dementia with parkinsonism linked to chromosome 17, and corticobasal degeneration (1). The etiological factors associated with neurodegenerative dementia include vascular, inflammatory, and metabolic factors. The most substantial overall risk factor for neurodegenerative dementia is aging. Aging of a population is associated with an increased incidence of AD, which affects more than 35 million individuals worldwide (2). The pathological features of AD are hyperphosphorylation of tau proteins in neuronal cells (leading to the formation of neuron fibrillary tangles (NFTs) (3)) and amyloid plaques (resulting from extracellular amyloid-beta [Aβ] deposition (4)). NFTs are associated with neuronal death and cognitive impairment (5).

Although tau is mainly an intraneuronal protein, autopsy analysis of the brain of patients with AD has revealed that the pathological impact of NFTs is stratified (6). The formation of NFTs is initiated at the transentorhinal cortex and subsequently develops in the synaptic areas of the brain, such as the hippocampus, or the new cortex (7). Previous studies have reported the aging-dependent roles of nuclear tau in neurodegeneration (8, 9). Recent studies indicated that tau, not Aβ, may be the key etiological factor for the symptoms of AD (10) and that tau deposits are a biomarker for monitoring AD (11), as well as tauopathies. Although many Aβ-targeted drugs in AD treatment have failed to show efficacy, the FDA recently approved one of the anti-Aβ antibodies to remove amyloid plaque from AD brains (12). For the other major AD pathological lesion, NFTs consisting of phosphorylated tau (p-tau) (13), and related research of tau-targeted treatment aiming to clear NFTs in AD brains also has appeared to be promising. It remains a formidable task to ensure that these targeted therapies have a demonstrated clinical efficacy.

The proteasome is reported to play an indispensable role in maintaining protein homeostasis and mediating neuronal apoptosis and synaptic plasticity (14–16). The accumulation of misfolded tau proteins, such as phosphorylated tau and NFTs, can impair the function of the 26S proteasome complex (3, 17), which increases the susceptibility of neurons to degeneration (18). *REGγ* codes for REGγ (also known as PA28γ, PSME3, Ki antigen, and the 11S family proteasome activator) (19), a noncanonical proteasome activator mediating ubiquitin-independent and ATP-independent protein degradation (20); it has been reported to decrease polyglutamine-expanded

‡ These authors contributed equally to this work.
* For correspondence: Jianru Xiao, jianruxiao83@163.com; Xiaotao Li, xiaotaol@gmail.com.

androgen receptor aggregation and consequently alleviate motor muscle atrophy and spinal and bulbar muscular atrophy (21). The expression of REGγ is upregulated in the neurons of human and mouse brains (22). Recent single cell RNA-seq and proteomic analyses have indicated that the expression of REGγ is markedly downregulated in aged individuals and patients with AD (23, 24). Consistent with these reports, bioinformatics analysis revealed that the expression of REGγ is downregulated in multiple tissues of patients with AD (25–27). The levels of REGγ were inversely correlated with those of tau. Thus, a panel of mutant REGγ derivative mice combined with the P301S Tg tau (PS19) model (3) was generated to elucidate the role of REGγ in AD. The PS19 model mouse has a transgenic human tau gene with a P to S change at position 301, a mutation found in human tauopathy. The findings of this study demonstrate that REGγ downregulation accelerates tau deposition and its effects, whereas the overexpression of REGγ ameliorates tau lesions in PS19 mice.

Results

Aging and age-related neurodegeneration conditions are associated with REGγ decline

Previously, we had reported that the depletion of REGγ in mice results in premature aging (28). Thus, in the present study, we aimed to evaluate REGγ expression patterns during aging and in age-related disorders. To determine REGγ profiles during physiological aging in mice, the REGγ expression levels were determined in mice aged 2 to 24 months (Figs. 1*A* and S1*A*). The levels of REGγ progressively decreased starting at the age of 5 months. Similar age-dependent reduction of REGγ was observed in the tauopathy model PS19. At 2 months of age, the expression of REGγ in PS19 mice was downregulated compared with that in the WT control (Figs. 1*A* and S1*A*). Next, bioinformatics analysis was performed to determine *REGγ* expression in the publicly available Gene Expression Omnibus (GEO) datasets of the National Center for Biotechnology Information database. The dataset comprised the gene expression profiles of postmortem AD brains. In particular, GSE1297 (26) (dataset 1) comprised 31 independent microarray data of nine healthy controls and 22 patients with AD, in which seven were severe cases. GSE159699 (27) (dataset 2) comprised the lateral temporal lobe RNA-seq analysis results of 12 patients with AD and 10 aged controls. Compared with those in the healthy controls, the *REGγ* mRNA levels were significantly downregulated in patients with AD. In particular, the *REGγ* mRNA levels were markedly downregulated in the hippocampal interneurons of patients with AD (Fig. 1*B*), with similar trends of *REGγ* decline in brain cortex and hippocampus in AD patients (Fig. S1*B*). To validate these findings, postmortem AD samples obtained from the Association of Human Brain Bank of China were subjected to immunohistochemical (IHC) analysis (29, 30). The expression of REGγ in the hippocampus of all five AD cases was markedly lower than that in the hippocampus of age-matched healthy controls (Fig. 1*C*). The staining of the same regions with anti-p-tau (AT8) antibodies revealed that the tau levels in AD specimens were significantly higher than those in healthy control specimens (Fig. 1*D*). This indicated that the levels of REGγ were inversely correlated with those of tau in the AD

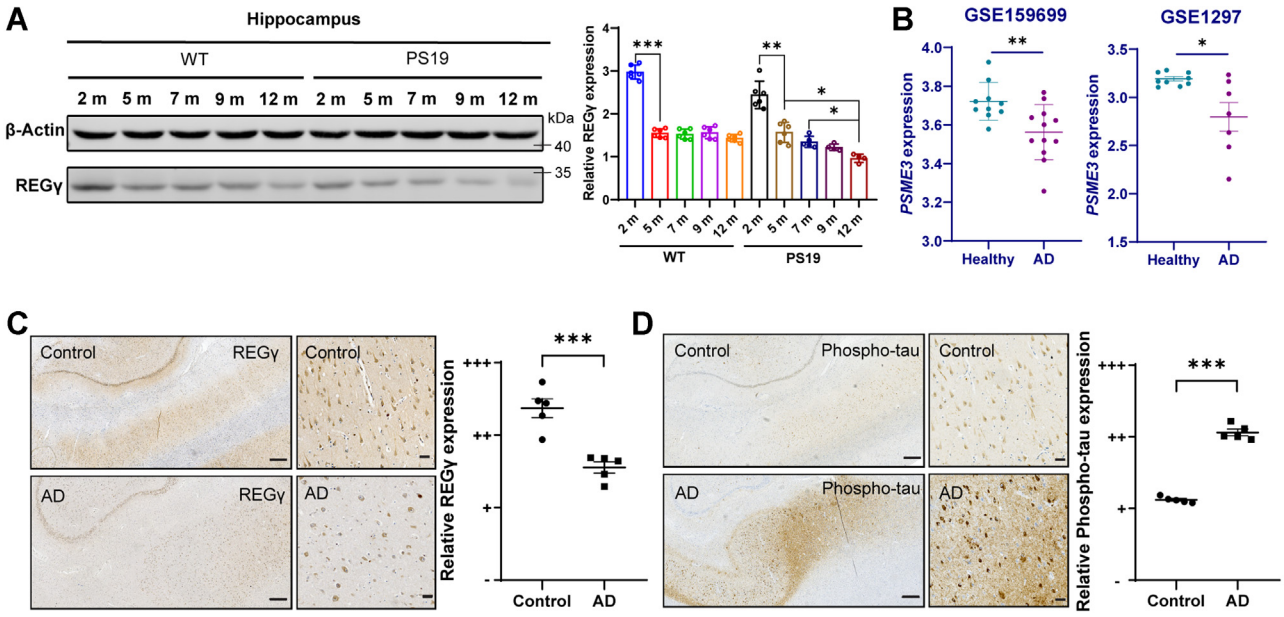

Figure 1. Aging and age-related neural degeneration are associated with REGγ decline. *A*, hippocampal tissues of WT and PS19 mice aged 2, 5, 7, 9, or 12 months were subjected to Western blotting. Quantitative analysis of REGγ expression in the hippocampus of young and aged WT and PS19 mice by one-way ANOVA. Data are represented as mean ± SD, *$p = 0.0232$, *$p = 0.0122$, **$p = 0.0086$, ***$p < 0.001$. *B*, Gene Expression Omnibus dataset analysis revealed that the *REGγ* mRNA levels in Alzheimer's disease (AD) tissues were downregulated compared with those in the healthy control tissues. Scatter plot of *REGγ* expression in healthy and AD samples in the GSE159699 (left) and GSE1297 (right) datasets. Gene expression is represented as $\log_2$ (FPKM+1). *C* and *D*, immunohistochemical staining of phospho-tau and REGγ in the hippocampal CA1 tissues of patients with AD and healthy controls. The scale bar represents 500 μm. The scale bar represents 50 μm in magnified images. Quantification of REGγ and phospho-tau immunostaining is shown on the *right side* of each panel. Data are represented as mean ± SEM (n = 5, two-tailed *t* test, ***$p < 0.001$).

brain lesions. These results suggest a potential role for REGγ in age-related dementia.

REGγ mediates ubiquitin-independent degradation of tau

To determine if REGγ regulates the levels of tau and p-tau, *REGγ* knockdown SH-SY5Y cell lines were established by transfecting cells with shRNA against *REGγ* (sh-REGγ or shR). Control shRNA (shN)–transfected cells were used as controls (31). The levels of tau (total tau/p-tau levels) were markedly higher in shR-transfected SH-SY5Y cells (Figs. 2*A*, left panel, Fig. S1*D*) and si-REGγ-transfected HT22 cells (Fig. 2*A*, right panel and Fig. S1*D*). However, transfection with shR and si-REGγ did not markedly affect the total *MAPT* or *mapt* mRNA levels, respectively (Fig. S1, *F* and *G*). Next, embryonic primary neuronal cells were isolated from the hippocampus of four different genotypes of mice for *in vitro* studies. The expression levels of human MAPT (in PS19 or P301S Tg, a mutant human Tau-overproducing mouse line) and mouse *mapt* (total tau/p-tau) were higher in the *REGγ* knockdown and *REGγ* KO;PS19 neurons (Figs. 2*B* and S1*E*), and a similar tendency displayed in mice brain hippocampus tissues (Fig. S2*A*). The degradation dynamics of tau and p-tau in shR-transfected and shN-transfected SH-SY5Y cells were analyzed in the presence of cycloheximide, a protein synthesis inhibitor. The decay of total tau (HT7) and p-tau (p-tau T231 and p-tau

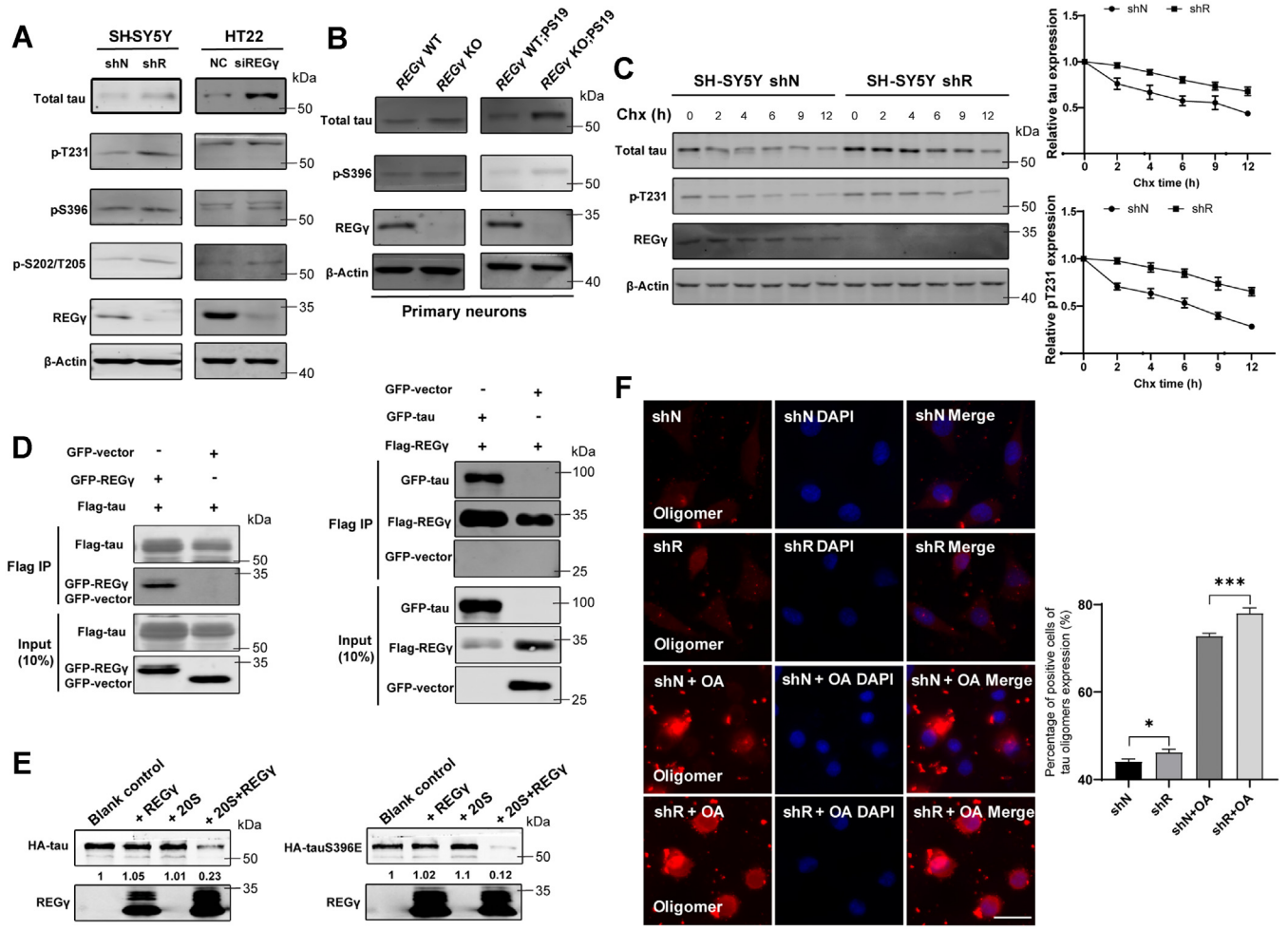

Figure 2. REGγ mediates ubiquitin-independent degradation of tau. *A*, *REGγ* was stably (using sh-REGγ) knocked down in human neuroblastoma cells (SH-SY5Y) or transiently (using si-REGγ) knocked down in mouse hippocampal neuron cells (HT22), which resulted in tau upregulation. The transfected cells were subjected to Western blotting. shN and NC indicate shRNA and siRNA controls, respectively. Quantitative analysis of relative protein expression normalized to actin control by two-tailed *t* test from (*A*) were shown in (Fig. S1*D*). *B*, Western blotting analysis of tau and p-tau levels in embryonic primary neuronal cells derived from the forebrain of *REGγ* WT, *REGγ* KO, *REGγ* WT;PS19, and *REGγ* KO;PS19 mice. Quantitative analyses of (*A* and *B*) were shown in Fig. S1, *D* and *E*. *C*, time course assay of cycloheximide (Chx) (100 μg/ml)-treated shN-transfected or shR-transfected SH-SY5Y cells. The expression levels were quantified using ImageJ and plotted to indicate dynamic changes, two-way ANOVA of total tau levels with shN/shR (n = 4, F = 23.57325, $^{**}p$ = 0.004653) and Chx treatment time (n = 4, F = 12.64963, $^{**}p$ = 0.007282) as the principal factors and the p-T231 levels with shN/shR (n = 4, F = 22.95905, $^{**}p$ = 0.00492) and Chx treatment time (n = 4, F = 8.226565, $^{*}p$ = 0.018621) as the principal factors. Data are represented as mean ± SEM. *D*, coimmunoprecipitation and Western blotting analyses revealed that exogenously expressed tau interacted with REGγ. Cotransfection of tau and REGγ containing Flag and GFP tags into the 293T cell line. *E*, *in vitro* proteolytic analyses were performed with purified REGγ, 20S proteasome, and *in vitro* translated tau for 3 h. *F*, REGγ-20S system degrades tau oligomers. Immunofluorescent staining of tau oligomers was performed in shN-transfected and shR-transfected SH-SY5Y cells before (serum starved for 12 h) and after okadaic acid (OA) (40 nM for 24 h) induction. Nuclei were stained with 4′,6-diamidino-2-phenylindole (DAPI; blue). The scale bar represents 20 μm. Quantitative results were analyzed by Wilcoxon test, n = 164, $^{*}p$ = 0.0485, $^{***}p < 0.001$. Data are represented as mean ± SEM. DAPI, 4′,6-diamidino-2-phenylindole.

S396) proteins in shR-transfected cells was markedly slower than that in the shN-transfected cells (Figs. 2*C* and S2*F*). This suggested that REGγ regulates the stability of tau and p-tau in these cells. Since identified REGγ substrate proteins must interact with the REGγ activator, the physical interaction between REGγ and tau proteins was examined using reciprocal coimmunoprecipitation assays with anti-REGγ, anti-total tau, or antihemagglutinin (HA)/GFP antibodies. Endogenous and exogenously expressed REGγ interacted with tau in cultured cells or hippocampus tissues of PS19 mice (Figs. 2*D* and S2, *B* and *C*). To determine the direct role of the REGγ-20S system in the degradation of tau and a mimic-phosphorylated tau, cell-free proteolysis was performed with purified proteins *in vitro*. Translated tau and tauS396E (a phosphorylation-mimetic mutant) were not significantly degraded upon incubation with 20S proteasome or REGγ (Fig. 2*E*; lanes 2 and 3). However, the combination of REGγ and 20S proteasome effectively degraded tau and tauS396E (Fig. 2*E*; lane 4). Soluble oligomers of tau protein are reportedly more toxic than the p-tau aggregates (32). We wondered if REGγ may also regulate the levels of soluble tau oligomers. Okadaic acid (OA), an efficient selective inhibitor of protein phosphatase 2A (PP2A) and protein phosphatase type 1 (PP1), was used to allow the accumulation of tau oligomers that can be recognized by a specific antibody (anti-Tau, T22) (33). The levels of soluble tau oligomers in OA-treated shR-transfected SH-SY5Y cells were 10% higher than those in OA-treated shN-transfected SH-SY5Y cells. This indicated that REGγ degrades soluble tau oligomers (Fig. 2*F*). These findings indicate that REGγ is directly involved in the degradation of multiple tau species in cells, as well as in a cell-free system.

The REGγ proteasome primarily targets phosphorylated nuclear tau for degradation

To elucidate the mechanism underlying REGγ proteasome-mediated turnover of phosphorylated tau, phosphorylation-mimetic (S396E and T231E) and phosphorylation-defective (S396A and T231A) mutant tau constructs were generated. Kinetic studies performed in the presence of cycloheximide revealed that the degradation of phosphorylation-mimetic tau mutants (S396E and T231E) in WT 293T cells was markedly faster than that in *REGγ* KO cells (34) (Figs. 3*A* and S2*G*). In contrast, the decay rates of phosphorylation-defective tau mutants (S396A and T231A) were similar in WT and *REGγ* KO 293T cells (Figs. 3*B* and S2*H*). This suggested that the REGγ proteasome primarily targets phosphorylated tau for degradation. REGγ, a nuclear protein, is thought to mediate the degradation of nuclear proteins, as well as the degradation of cytoplasmic proteins that shuttle between cytosol and nuclei (35). Next, we investigated the effect of phosphorylation on the cellular distribution of tau in SH-SY5Y cells. OA treatment promoted the nuclear localization of tau in more than 90% of the cells (Fig. 3*C*), suggesting a role of phosphorylation in the nuclear translocation of tau. To test this, WT tau or phosphorylation-mimetic/defective tau (with a single mutation) constructs were generated and exogenously expressed in WT or *REGγ*-deficient cells. The nuclear translocation of WT human tau in REGγ-deficient cells was approximately 50% more than that in WT controls (Fig. 3*D*). The expression of phosphorylation-mimetic tau enhanced the nuclear translocation of tau by approximately 90%. In contrast, transfection with phosphorylation-defective tau did not affect its nuclear translocation (Figs. 3, *E* and *F* and S2*E*). Consistent with the immunostaining results, the expression of WT tau or phosphorylation-mimetic tau (but not that of phosphorylation-defective tau) in REGγ-deficient cells was upregulated compared with that in control cells (Fig. S2*D*). These findings suggest the nuclear translocation of phosphorylated tau may explain the reason for REGγ primarily mediating the degradation of nuclear tau.

Gain or loss of REGγ function differentially regulates tau accumulation in vivo

To investigate REGγ-mediated regulation of tau *in vivo*, transgenic mice with forebrain neuron-specific overexpression of REGγ were generated after crossing *REGγ* knock-in allele (KI) mice with Camk2α-cre mice (Fig. S3*A*). *REGγ* KI mice were obtained without any changes in the brain REGγ level compared to the *REGγ* WT; thus, either mouse group could be used as REGγ normal controls. Thus *REGγ* KI and *REGγ* WT mice were used as control mice for *REGγ* KO and *REGγ* OE mice. Similarly, the mice in the PS19 group, *REGγ* KI;PS19, and *REGγ* WT;PS19 were used as the control group against *REGγ* KO;PS19 and *REGγ* OE;PS19 mice. *REGγ* KI and *REGγ* WT mice were crossed with PS19 mice to generate Control;PS19 mice with the same REGγ levels. Quantitative real-time PCR (qRT-PCR) analysis revealed that the *REGγ* levels were highest in the hippocampus and cortex of Camk2α-cre mice with homozygous *REGγ* KI (Homo-*REGγ* OE). However, the *REGγ* level in the cerebellum of Camk2α-cre mice with heterozygous *REGγ* KI (Hetero-*REGγ* OE) or Homo-*REGγ* OE mice were not upregulated compared with that in the cerebellum of the controls (Fig. S3, *B*–*D*). This was consistent with the expectation that Camk2α-cre drives REGγ expression in forebrain neurons. To validate the conditional expression of the Flag-REGγ KI allele, homogenized forebrain tissues (*REGγ* OE mice forebrain tissues) were immunoprecipitated with anti-Flag antibodies. Mass spectrum analysis revealed the expression of exogenous *REGγ* alleles in the mouse brain (Fig. S3*E*). IHC analysis with anti-Flag (left and middle panels) or anti-REGγ (right panel) antibodies revealed the differential expression of REGγ in the hippocampus of REGγ-overexpressing and normal control mice (Fig. S3*F*). Next, the *REGγ* KO or *REGγ* OE mice were crossed with PS19 mice to generate *REGγ* KO;PS19 or *REGγ* OE;PS19 mice, respectively. To examine the effects of REGγ levels on various tau species *in vivo*, the hippocampal tissues of mice aged 8 and 10 months from the six different genotypes were analyzed by Western blotting analysis with p-tau–specific antibodies. The total tau (HT7) and p-tau (pS396 and pT231) levels in both *REGγ* KO and *REGγ* KO;PS19 (human tau species with slower migration) mice were significantly higher compared with those in Control

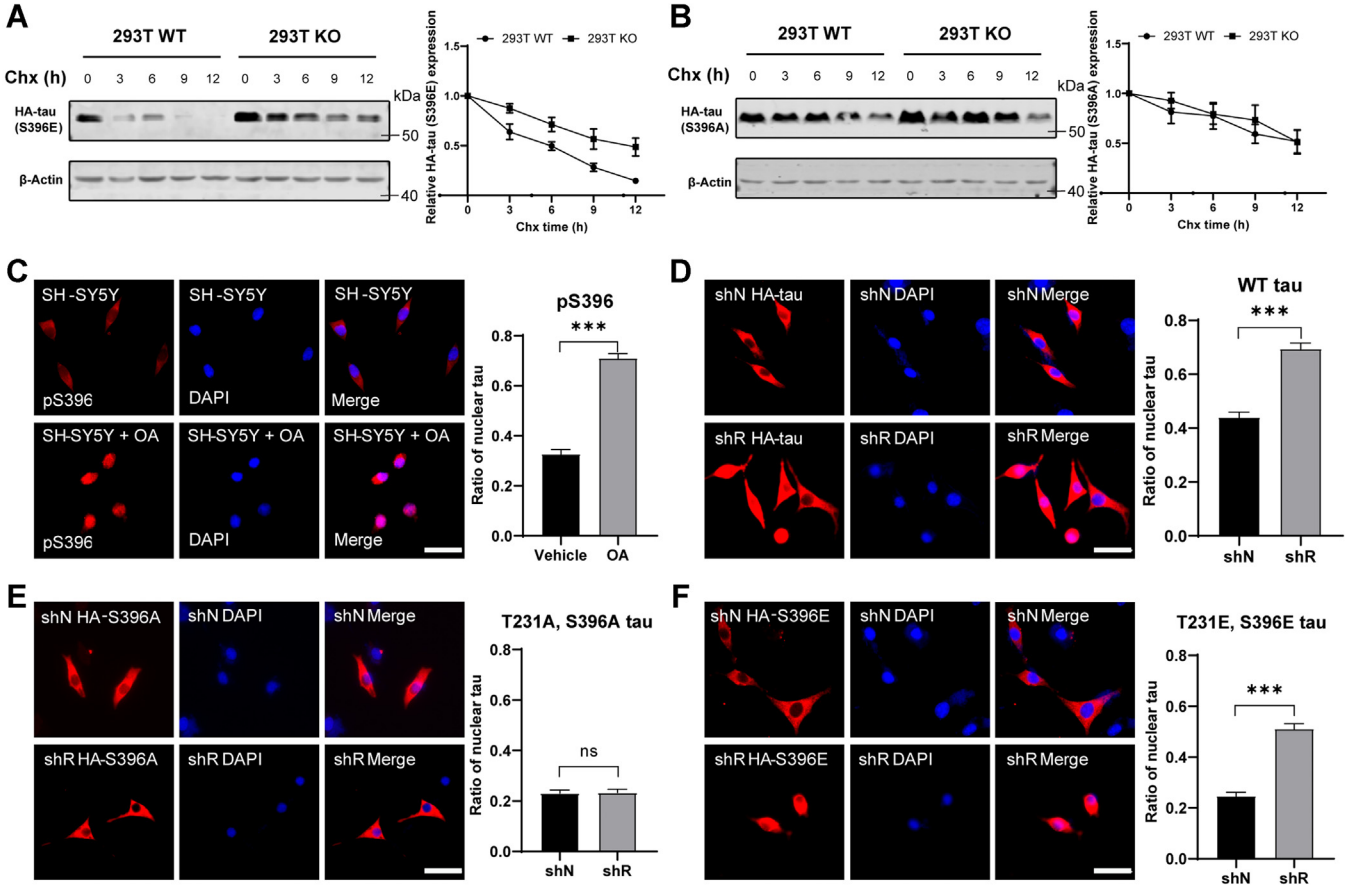

Figure 3. REGγ primarily targets nuclear phosphorylated tau for degradation. *A*, hemagglutinin (HA)-tagged tau (S396E) was transfected into WT and *REGγ* KO 293T cells for 24 h, treated with cycloheximide (Chx) (100 μg/ml) for the indicated duration, and subjected to Western blotting. Quantitative results of HA-tau (S396E) stability were plotted to indicate the dynamic changes. Two-way ANOVA of the HA-tau (S396E) group results with WT/*REGγ* KO 293T cells (n = 6, F = 13.86929, $*p = 0.020401$) and Chx treatment time (n = 6, F = 17.53975, $**p = 0.008414$) as the principal factors. *B*, the 293T cells were transfected with phosphorylation-defective mutant HA-tau (S396A) and treated as in (*A*). Quantitative results of HA-tau (S396A) stability were plotted to indicate the dynamic changes. Two-way ANOVA of the HA-tau (S396A) group results with WT/*REGγ* KO 293T cells (n = 6, F = 3.082835, $p = 0.15397$) and Chx treatment time (n = 6, F = 30.49188, $**p = 0.002961$) as the principal factors. *C*, immunofluorescent staining of p-tau S396 in SH-SY5Y cells before (serum-starved for 12 h) and after OA (40 nM for 24 h)-induced tau phosphorylation. Nuclei were stained with DAPI (*blue*). The scale bar represents 20 μm. Quantitative results were calculated by Wilcoxon test, n = 198, $***p < 0.001$. Data are represented as mean ± SEM. *D–F*, HA-tau, HA-tau (S396A), and HA-tau (S396E) were separately transfected into control shRNA-transfected (shN) and sh-REGγ-transfected (shR) SH-SY5Y cells. The cells were then stained with anti-HA (*red*) antibodies and DAPI (*blue*). The scale bar represents 20 μm. At least 200 cells of each sample were analyzed in triplicate with Wilcoxon test. Data are represented as mean ± SEM. $***p < 0.001$. All data are representative of three independent repeats. DAPI, 4′,6-diamidino-2-phenylindole.

or Control;PS19 (Fig. 4, *A* and *D*). Increased p-S202/T205 (AT8) staining intensity was only observed in *REGγ* KO;PS19 mice (Fig. 4*A*) but not in Control;PS19 mice. This suggested that REGγ depletion promotes tau hyperphosphorylation in PS19 mice. In contrast, the hippocampus of *REGγ* OE;PS19 mice exhibited significantly lower expression of total tau (HT7) and p-tau (detected using p-T212/S214 [AT100]) and AT8 than that of Control;PS19 mice (Fig. 4, *B–D*). Tau is reported to accumulate with aging in the neurons of the hippocampus and is concomitantly downregulated in tau immune-reactive CA3 mossy fibers (3). The results of this study were consistent with this observation (see arrow heads in Fig. 4*E*). Comparison of the tau staining revealed the levels of nuclear tau in *REGγ* KO;PS19 and *REGγ* OE;PS19 mice (Fig. 4*G*). Our findings of higher levels in the KO were consistent with the observation in cultured cells treated with OA (Fig. 3*C*) or expression of phosphorylation-mimetic tau (Fig. 3*F*). IHC analysis revealed that p-tau stained with T231 (AT180) or AT8 antibodies was markedly upregulated in *REGγ* KO;PS19 but downregulated in *REGγ* OE;PS19 mice (Figs. 4*F* and S3*G*). These findings were consistent with those of Western blotting analysis (Fig. 4, *A–D*) and demonstrate the effects of REGγ on tau protein levels.

REGγ deficiency promotes neurodegeneration

To evaluate the effect of REGγ levels on brain atrophy and cytoarchitecture in PS19 models, computer-assisted image analysis of brain size and the number of neurons in CA1 regions in mice belonging to the six different genotypes was performed. The size of the whole brain and hippocampus was not remarkably different among Control, *REGγ* KO, and *REGγ* OE mice aged 10 months. In contrast, Control;PS19 mice exhibited marked brain atrophy, while ventricular dilation was observed in age-matched *REGγ* KO;PS19 mice. These pathological changes were alleviated in *REGγ* OE;PS19 mice

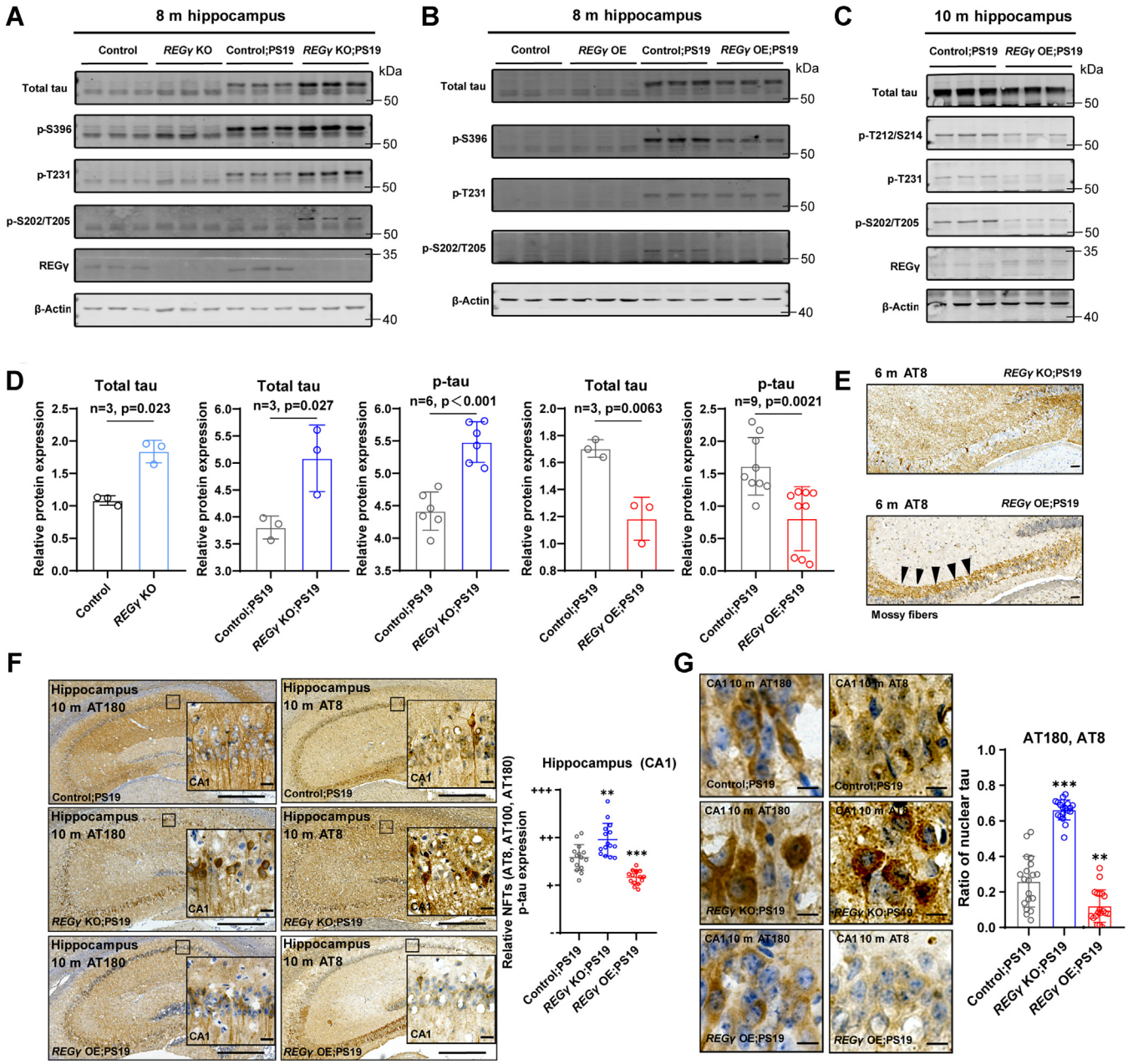

Figure 4. Gain or loss of REGγ function differentially regulates tau accumulation *in vivo*. *A–C*, overexpressing REGγ in the neurons downregulated the tau and p-tau levels in the hippocampal tissues of mice with or without REGγ depletion. The hippocampal tissues of Control, *REGγ* KO, *REGγ* overexpressing (OE), Control;PS19, *REGγ* KO;PS19, and *REGγ* OE;PS19 mice aged 8 and 10 months were subjected to Western blotting analysis. And the quantitative analysis of relative protein expression normalized to actin control by two-tailed *t* test from (*A–C*) were shown in (*D*). Data are represented as mean ± SD. *E*, immunohistochemical staining by AT8 in the hippocampal tissues of *REGγ* KO;PS19 and *REGγ* OE;PS19 mice aged 10 months. *Arrows* indicate the mossy fibers. The scale bar represents 20 μm. *F*, immunohistochemical staining by AT180 and AT8 (neurofibrillary tangles [NFTs]) in the hippocampal tissues of Control;PS19, *REGγ* KO;PS19, and *REGγ* OE;PS19 mice aged 10 months. Background hippocampus scale bar is 500 μm. Magnified images indicate the CA1 regions. The scale bar represents 50 μm. Quantitative immunohistochemical analysis results of NFTs (including AT8, AT100, and AT180) in the CA1 area of different groups by one-way ANOVA, n = 15, $^{**}p = 0.0011$, $^{***}p < 0.001$. Data are represented as mean ± SD. *G*, respective CA1 region from (*F*) was magnified to show p-tau nuclear expression in REGγ-deficient mice. The scale bar represents 10 μm. Quantitative results of nuclear p-tau (AT8 and AT180 included) expression in the CA1 regions of different groups by one-way ANOVA, n = 19, $^{**}p = 0.0038$, $^{***}p < 0.001$. Data are represented as mean ± SD.

(Fig. 5*A*). Nissl staining analysis of the neuron layer thickness in the hippocampus revealed an increased neuron degeneration in PS19 (Control;PS19) mice aged 10 months that was further exacerbated (thinner) in *REGγ* KO;PS19 mice but significantly alleviated in *REGγ* OE;PS19 mice (Fig. 5*A*, lower panel). The density of neurons in PS19 and *REGγ* KO mice appeared to be less than that in Control and *REGγ* OE mice. To determine the neuronal loss in the CA1 regions, the brains of the different mouse genotypes were stained with anti-NeuN antibodies. Quantitative analysis of CA1 regions revealed 69% and 44% of control neurons in *REGγ* KO and *REGγ* KO;PS19 mice, respectively (Fig. 5*B*). Mice with compound mutations in REGγ and tau (*REGγ* KO;PS19) exhibited more than 50% loss in CA1 neurons, which was significantly alleviated in *REGγ*

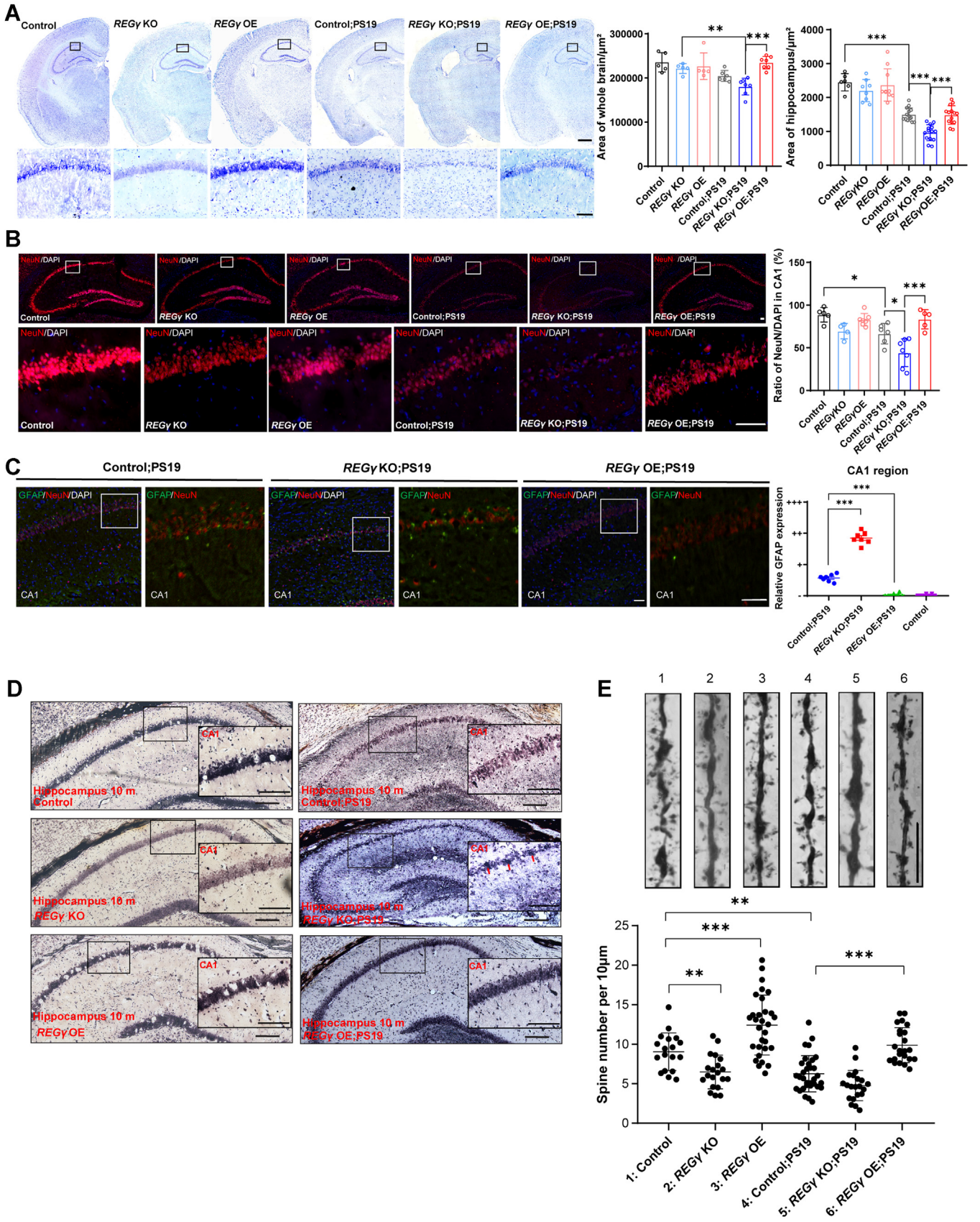

Figure 5. REGγ overexpression mitigates REGγ deficiency-mediated neurodegeneration. *A*, nissl staining of the whole brains of mice aged 10 months. The scale bar represents 50 μm. The magnified images indicate the CA1 regions (*squares*). The scale bar represents 20 μm. Quantitative analysis of the area of whole brain and the hippocampus was performed with computerized scanning. Two-way ANOVA of whole brain area and hippocampus area with REGγ and PS19 as the principal factors, $^{**}p = 0.0093$, $^{***}p < 0.001$. Data are represented as mean ± SD. *B*, hippocampal regions of different groups were stained

OE;PS19 mice (Fig. 5*B*). We found similar changes in dentate gyrus regions of corresponding mice (Fig. S3, *H* and *I*). Gliosis is associated with tau lesions and/or neuronal loss in tauopathies (36, 37). Hence, mouse brains from different genotypes were stained using anti-glial fibrillary acidic protein (GFAP) antibodies. GFAP signals were observed throughout the whole brain of PS19 mice. We also found increased GFAP staining in the white and gray matter of the hippocampus and other brain regions in *REGγ* KO;PS19 (Fig. 5*C*). The levels of GFAP were significantly attenuated in *REGγ* OE;PS19 (Fig. 5*C*). This suggested a reduction in astrogliosis, which may be due to attenuated tau lesions and neuron loss. Consistent with these observations, Gallyas–Braak silver staining revealed that the number of NFTs (red arrow heads) in *REGγ* KO;PS19 mice was more than that in Control;PS19 or *REGγ* OE;PS19 mice (Fig. 5*D*). Loss of synapse formation is reported to be an early marker in the PS19 tauopathy model (3). Golgi staining was performed to analyze the dendritic spines in the cortex. The results of all animals in each genotype were averaged. Compared to Control mice, the number of dendritic spines was lower in *REGγ* KO mice and further decreased in *REGγ* KO;PS19 mice (Fig. 5*E*). The dendrite abnormality in *REGγ* KO;PS19 mice was alleviated with increased spine density in *REGγ* OE;PS19 mice (Fig. 5*E*). These results suggest that loss of REGγ potentiates neurodegenerative phenotypes in PS19, and these changes can be alleviated by restoring REGγ function.

Restoring REGγ expression alleviates tauopathy-associated behavioral and cognitive impairments

Impaired learning and memory are the hallmarks of human tauopathy. Previously, we had reported the effect of REGγ levels on the hippocampus-dependent spatial memory using the Morris water maze test (38). Mice belonging to six different genotypes without significant differences in swimming speed or motor activity were screened out (Fig. S4, *A* and *B*). The learning of 6-month-old and 9-month-old *REGγ* OE;PS19 mice was faster than that of Control;PS19 and *REGγ* KO;PS19 mice (Fig. S4*C*). The percentage of time spent in the target quadrant and the number of times to the hidden platform by *REGγ* OE mice were significantly higher than those by Control and *REGγ* KO littermates. Similarly, the percentage of time spent in the target quadrant and the number of visits to the platform by *REGγ* OE;PS19 mice were higher than those in Control;PS19 and *REGγ* KO;PS19 mice (Figs. 6*A* and S4*E*). During the reversal probe trial in which the target platform was switched to the opposite quadrant, the learning of latency to reversal platform of *REGγ* OE;PS19 mice was faster than that of Control;PS19 and *REGγ* KO;PS19 mice (Fig. S4*D*). Moreover, Control;PS19 and *REGγ* KO mice spent an increased amount of time in the primary platform target quadrant and decreased amount of time in the reversal quadrant (Fig. 6*B*). Spatial learning ability was examined using the radial eight-arm maze task (39). Overexpression of REGγ decreased the number of errors in both REGγ-deficient and PS19 mice, including *REGγ* KO;PS19 mice (Fig. 6*C*). These results indicate that REGγ is crucial for hippocampus-dependent spatial memory. To further examine the effect of REGγ dysfunction on cognitive and noncognitive (such as anxiety and motivation) impairments in Control;PS19 mice, novel object recognition (NOR) (to evaluate the hippocampus-dependent short-term memory) and elevated plus maze (EPM) tests were performed. In mice exhibiting a similar discrimination index for objects A and B, the novel object index (NOI) was measured before and after switching object B to a different object C. The NOIs of *REGγ* OE;PS19 mice were significantly higher than those of *REGγ* KO;PS19 littermates (Fig. S4*F*). EPM was used to investigate anxiety based on the natural spontaneous exploratory behavior of mice in novel environments, as well as on their natural aversion for elevated and open areas, and the tau mutant transgenic mice spent more time in the open arms, indicating that their anxiety might be lower (40). The anxiety levels in *REGγ* OE;PS19 mice were significantly higher than those in Control;PS19 and *REGγ* KO;PS19 mice, indicating that REGγ activity can prevent anxiety behavior in the mouse models (Fig. 6*D*). In addition to the beneficial effect of *REGγ* overexpression on neurodegenerative phenotypes in PS19 mice (*REGγ* OE;PS19 mice), the life span of *REGγ* OE;PS19 mice was significantly longer than that of Control;PS19 and *REGγ* KO;PS19 mice (Figs. 6*E* and S4*G*). These results demonstrate that increased REGγ activity alleviates tauopathy-induced cognitive deficits and promotes prolonged survival of mice.

Potential mechanisms involved in aging-associated and tauopathy-associated REGγ reduction

To determine if the reduced REGγ expression in aged and AD/tauopathy brains (Fig. 1) resulted from dysregulation or loss of neurons, transcriptional regulation of *REGγ* in neuronal cells was examined *in vivo* and *in vitro*. CCAAT enhancer-binding protein-beta (C/EBPβ), a transcription factor that is activated in response to inflammation regulates a panel of factors, such as δ-secretase and apolipoprotein E ε4 (APOE4) (41, 42) C/EBPβ, is upregulated in the aged brain (43) and is reportedly a factor that induces cognition defects in mice (44). Transforming growth factor beta receptor (TGFβR), which is a

with anti-NeuN (*red*) antibodies and DAPI (*blue*); *blue*. Magnified images indicate the CA1 areas (in *squares*). The scale bar represents 20 μm. Quantitative analysis of NeuN expression relative to DAPI intensity. Two-way ANOVA of relative NeuN expression with REGγ and PS19 as the principal factors, $^{*}p_{(\text{Control } versus \text{ Control;PS19})} = 0.0346$, $^{*}p_{(\text{Control;PS19 } versus \text{ REGγ KO;PS19})} = 0.0168$, $^{***}p < 0.001$. Data are represented as mean ± SD. *C*, immunofluorescent staining of GFAP (*green*) and NeuN (*red*) in the hippocampal CA1 region of mice aged 10 months. The scale bar represents 20 μm. Quantitative analysis of GFAP in the CA1 region of different groups by two-tailed *t* test, $^{***}p < 0.001$. Data are represented as mean ± SEM. *D*, the hippocampal tissues of Control, *REGγ* KO, *REGγ* overexpressing (OE), Control;PS19, *REGγ* KO;PS19, and *REGγ* OE;PS19 mice aged 10 months were subjected to Gallyas–Braak silver staining. Background hippocampus scale bar is 200 μm. Magnified images indicate the CA1 regions (*squares*). *Red arrows* indicate neurofibrillary tangles. The scale bar represents 50 μm. *E*, the brain sections of transgenic mice were subjected to Golgi staining to examine the apical dendritic layer of the CA1 region. The scale bar represents 10 μm. Quantitative analysis of spine density in different groups by one-way ANOVA. Data are represented as mean ± SD. $^{*}p < 0.05$, $^{**}p < 0.01$, and $^{***}p < 0.001$. All data are representative of three independent repeats. DAPI, 4′,6-diamidino-2-phenylindole.

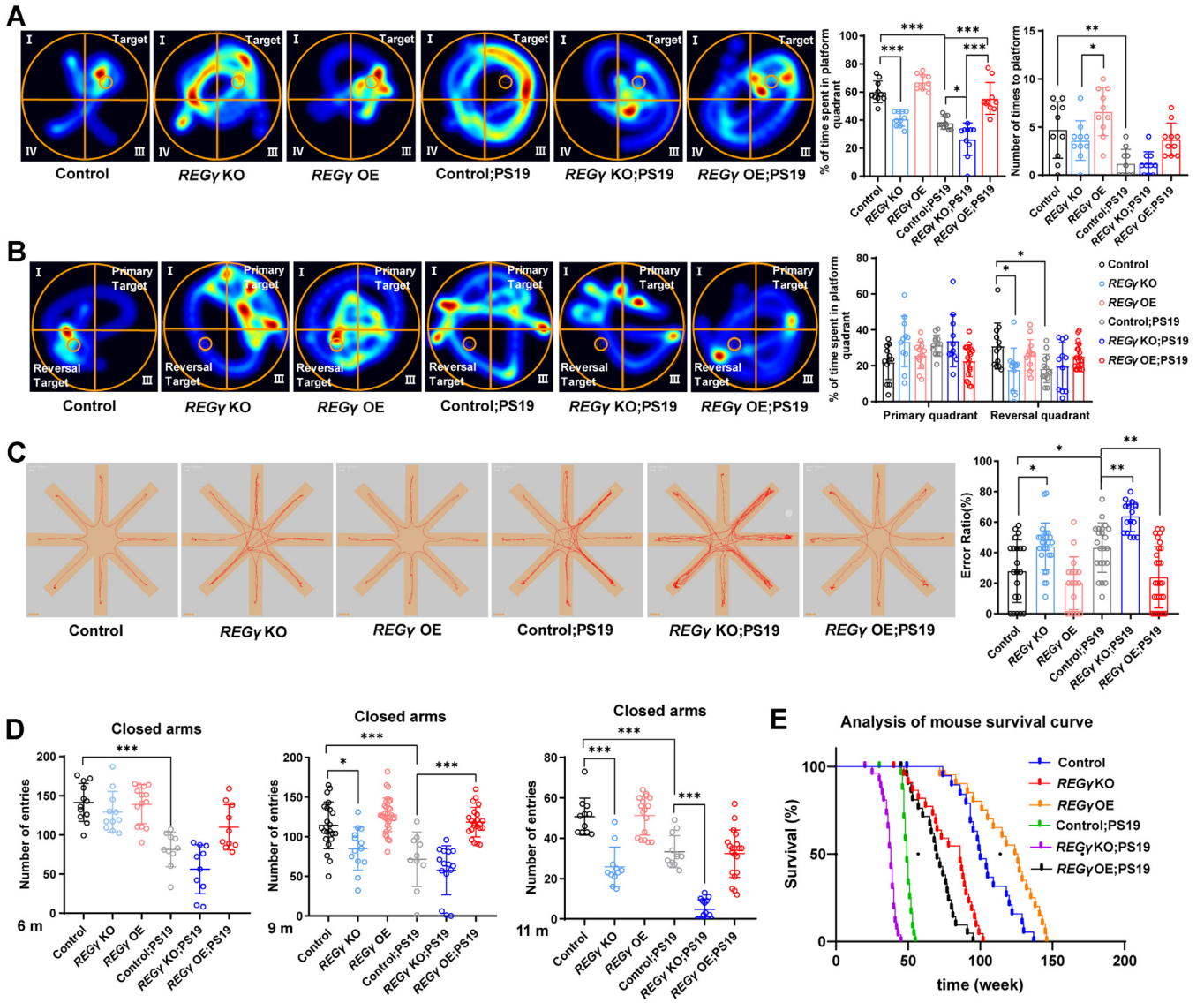

Figure 6. Restoration of REGγ expression alleviates tauopathy-induced behavioral and cognitive impairments. *A*, swimming traces of 6-month-old Control, *REGγ* KO, *REGγ* overexpressing (OE), Control;PS19, *REGγ* KO;PS19, and *REGγ* OE;PS19 mice and the percentage of time spent in the target quadrant during the Morris water maze probe trials (solid bar graph; n = 10/group; mean ± SD; $^{*}p = 0.026$,$^{***}p < 0.001$; two-way ANOVA with REGγ and PS19 as the principal factors). Open bar graph shows the number of times to platform (n = 10/group; Data are represented as mean ± SD; $^{*}p = 0.0241$, $^{**}p = 0.0051$; two-way ANOVA with REGγ and PS19 as the principal factors). *B*, swimming traces of 9-month-old transgenic mice during the reversal probe trials. Quantitative results on the right shows the percentage of time spent in the primary and reversal target quadrants by 9-month-old males Control (n = 12), *REGγ* KO (n = 11), *REGγ* OE (n = 13), Control;PS19 (n = 13), *REGγ* KO;PS19 (n = 11), and *REGγ* OE;PS19 (n = 19) mice (mean ± SD; $^{*}p_{(REGγ\ KO\ versus\ Control)} = 0.0305$, $^{*}p_{(Control;PS19\ versus\ Control)} = 0.0326$ in the reversal quadrant; two-way ANOVA with REGγ and PS19 as the principal factors). *C*, route taken by 9-month-old males and the error ratio (mean percentage of repeat visits into the same arm) in the eight-arm radial maze. Control (n = 21), *REGγ* KO (n = 26), *REGγ* OE (n = 17), Control;PS19 (n = 22), *REGγ* KO;PS19 (n = 17), and *REGγ* OE;PS19 mice (n = 28) (mean ± SD; $^{*}p_{(REGγ\ KO\ versus\ Control)} = 0.0202$, $^{*}p_{(Control;PS19\ versus\ Control)} = 0.0463$, $^{**}p_{(REGγ\ KO;PS19\ versus\ Control;PS19)} = 0.0045$, and $^{**}p_{(REGγ\ OE;PS19\ versus\ Control;PS19)} = 0.0019$; two-way ANOVA with REGγ and PS19 as the principal factors). *D*, the number of entries to the closed arms in the elevated plus maze tests by transgenic mice aged 6, 9, or 11 months. Data are represented as mean ± SD. $^{*}p = 0.0179$, $^{***}p < 0.001$; two-way ANOVA with REGγ and PS19 as the principal factors. *E*, Kaplan–Meier analysis of Control (n = 20), *REGγ* KO (n = 23), *REGγ* OE (n = 19), Control;PS19 (n = 25), *REGγ* KO;PS19 (n = 27), and *REGγ* OE;PS19 (n = 22) mice. Survival rate curves were generated using the Kaplan–Meier method and the *p* values (see Supplementary) were calculated using the two-tailed log-rank (Mantel-Cox) test.

transcription target of C/EBPβ (45), mediates a signaling pathway to repress transcription of *REGγ* (46). Compared with that in the hippocampal tissues of 24-month-old mice, the *REGγ* mRNA levels were downregulated and the *Cebpb* and *Tgfbr2* mRNA levels were upregulated in the hippocampal tissues of 3-month-old mice (Fig. 7*A*). Furthermore, transfection of CEBPB into SH-SY5Y cells upregulated the expression of *TGFBR2* and significantly downregulated the *REGγ* levels (Figs. 7*B* and S1*C*). These results suggest that age-dependent reduction of REGγ may result from dysregulation of the C/EBPβ signaling pathway.

Based on the findings of this study, we propose a model for the role of the proteasome activator REGγ in the regulation of tau homeostasis. The REGγ-20S system degrades tau species, including tau oligomers. Genetic ablation of REGγ promotes tauopathies in PS19 models, whereas conditional activation of

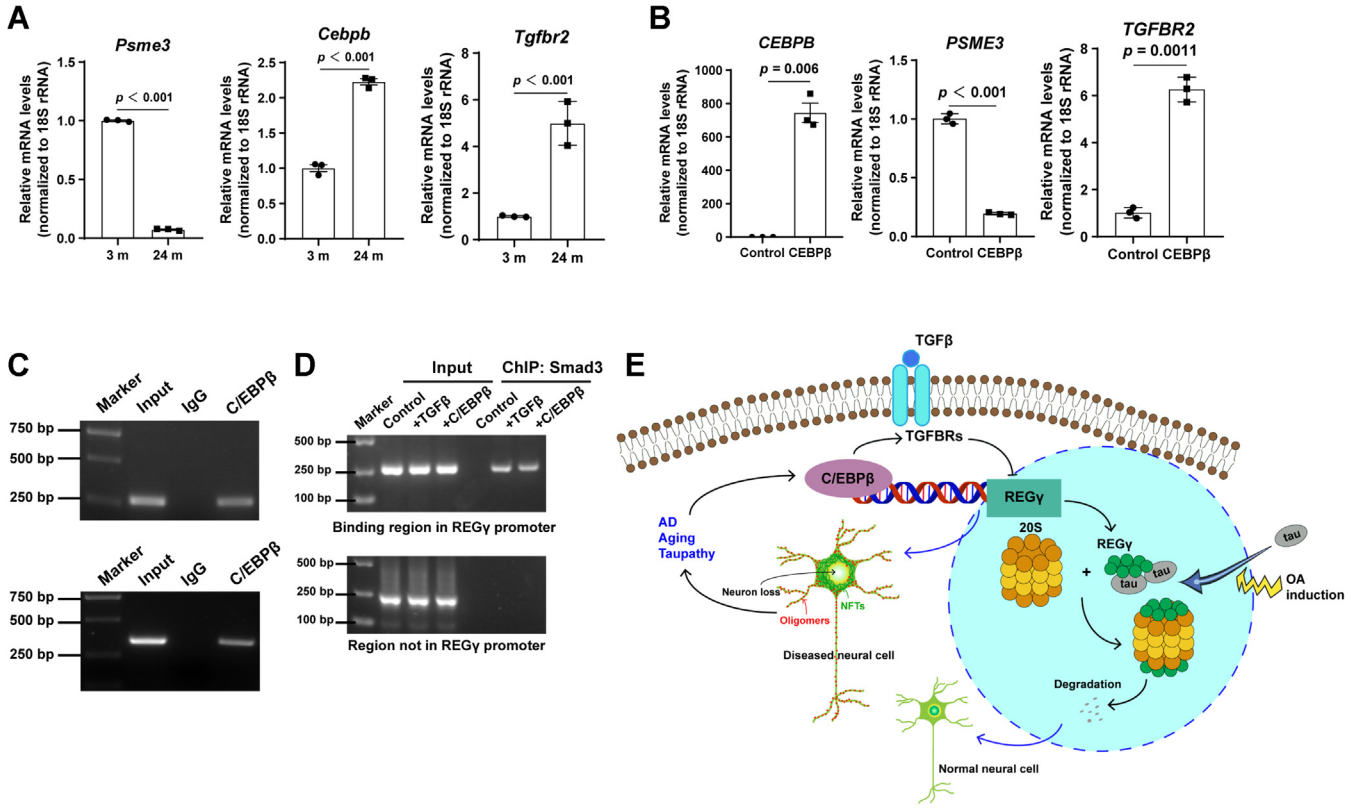

Figure 7. A schematic model for the pathway involved in the regulation of REGγ and tau. *A*, *Psme3* mRNA level was downregulated in the hippocampal tissues of mice aged 24 months with a concomitant upregulation of *Cebpb* and *Tgfbr2* mRNA levels. Hippocampal tissues of mice aged 24 and 3 months were subjected to quantitative real-time PCR (qRT-PCR) analysis. Relative mRNA levels of these factors were compared between tissues from 3-month-old and 24-month-old mice (mean ± SEM; n = 3; ***$p < 0.001$; 3 m *versus* 24 m). *B*, transient expression of CEBPB upregulated the *TGFBR2* mRNA levels and downregulated the *PSME3* mRNA levels in SH-SY5Y cells. SH-SY5Y cells transfected with CEBPB-encoding or control plasmid were subjected to qRT-PCR to determine the levels of the indicated genes. Data are represented as mean ± SEM from three independent experiments (**$p < 0.01$ and ***$p < 0.001$. CEBPB-transfected group *versus* control-transfected group). All data are representative of three independent repeats. *C*, ChIP assays were performed to substantiate *in vivo* binding of C/EBPβ to the TGFβR2 promoter in SH-SY5Y cell line, two pairs of primers in the binding enrichment locus were used (upper and lower panels). *D*, ChIP assays were performed to substantiate *in vivo* binding of Smad3 to the REGγ promoter in SH-SY5Y cell line with TGFβ or C/EBPβ, two pairs of primers (*upper panel* is for Smad3-binding region in REGγ promoter, *lower panel* is ∼2 Kb upstream of REGγ promoter). *E*, a model depicting the regulation of REGγ and tau. Highly activated C/EBPβ in senescent cells, such as those in AD, aging, and tauopathy are associated with a concomitant upregulation of TGFBRs, especially TGFBR2. TGFβ signaling may promote REGγ downregulation. Lack of REGγ promotes the accumulation of tau and p-tau, which leads to tau hyperphosphorylation, formation of neurofibrillary tangles and tau oligomers, and neuron loss in neurodegenerative mouse models. ChIP, chromatin immunoprecipitation.

REGγ expression in the forebrain neurons rescues tau lesion and aging-associated neurodegenerative phenotypes. With age, C/EBPβ signaling activation leads to a decline in the levels of *REGγ* in association with inflammation. Concomitantly, the loss of REGγ promotes the nuclear translocation of tau, which may promote pathological function of tau other than aggregates.

Overexpression of CEBPB in human neuroblastoma cells (SH-SY5Y cell) downregulated the *REGγ* mRNA levels and upregulated the *TGFBR2* mRNA levels (Figs. 7*B* and S1*C*). Moreover, binding of C/EBPβ to the TGFβR2 locus has been reported in the chromatin immunoprecipitation (ChIP) sequencing database in human A549 cell line. ChIP assays performed in the SH-SY5Y cell line indicated that C/EBPβ could be recruited to the TGFβR2 promoter in a neuronal cell line (Fig. 7*C*). C/EBPβ-induced activation of TGFβ signaling *via* promotion of TGFβR2 was evidenced by enriched Smad3 on *REGγ* promoter, but not in regions further upstream, by ChIP analyses in SH-SY5Y cell line (Fig. 7*D*). Compared with those in the brain hippocampus of 3-month-old mice, the *Cebpb* and *Tgfbr2* levels in 24-month-old mice were upregulated and the *REGγ* levels were markedly downregulated in the brain (Fig. 7*A*). Therefore, age-related REGγ reduction appears to be regulated by C/EBPβ through the TGFβ signaling pathway. The findings of this study may be clinically relevant for the development of new therapeutic strategies for neurodegenerative diseases, such as tauopathies and AD.

Discussion

This study demonstrated that REGγ plays a critical role in the regulation of hippocampus-dependent learning and memory in AD-like syndromes by directly targeting tau and p-tau for proteasome-mediated degradation. REGγ deficiency markedly upregulated the levels of phosphorylated tau in the nuclei, promoted the accumulation of toxic tau oligomers, and consequently potentiated neurodegenerative tauopathy in mouse models. This study presents proof-of-principle

evidence for neuron-specific REGγ expression-mediated mitigation of the progression of tauopathy or AD-like symptoms. Mechanistic studies led to a proposed link between aging-associated REGγ downregulation and tau-related neurodegeneration (Fig. 7*E*).

We found that aging and aging-associated degenerative dementia were associated with downregulated REGγ expression. This is consistent with the results of a previous study, which reported that REGγ deficiency promotes premature aging in mice (28). The findings of this study are consistent with those of a previous study (47). Additionally, this study demonstrates that the mRNA and protein levels of REGγ were upregulated in the pyramidal neurons of healthy brain regions, including the hippocampus (Allen Brain Institute https://mouse.brain-map.org/ and the Human Protein Atlas Institute http://www.proteinatlas.org/). Previously, we had proposed a mechanism through which REGγ is downregulated by C/EBPβ (43) *via* the TGFβ (46) signaling pathway. However, we do not exclude the possibility of additional factors contributing to aging-associated REGγ reduction.

To the best of our knowledge, this is the first study to report the degradation of tau and p-tau proteins by the ubiquitin-independent REGγ-proteasome system. Various tau clearance pathways have been previously reported. The major intracellular degradation processes are ubiquitin-proteasome system (UPS) and autophagy (48). These tau degradation pathways can act on different forms of tau protein. Excessive soluble neurotoxic tau proteins can be degraded through the UPS (49), chaperon-mediated autophagy (50), and endosomal microautophagy (51). Meanwhile, the intraneuronal insoluble tau is degraded *via* macroautophagy (52). Based on our previous results, all the substrate proteins identified to be targeted by the REGγ-proteasome system are also regulated by UPS. In most cases, UPS mediates signal-mediated acute degradation of protein substrates, whereas the REGγ-proteasome system primarily maintains the steady state levels of these proteins. We believe the ubiquitin-dependent and ubiquitin-independent regulation of tau will be orchestrated in similar fashion under normal conditions. However, both UPS and autophagy pathways are impaired in several neurodegenerative diseases (53, 54). This suggests the importance of the REGγ pathway in the maintenance of the homeostasis of key cellular proteins including tau proteins. The identification of REGγ-mediated tau degradation provides additional therapeutic targets for aging-associated neurodegeneration.

For more than 3 decades, Tau proteins have been reported to localize to the neuronal and non-neuronal cell cytoplasm, as well as to the nucleus, (8). However, most studies have focused on the role of tau in the physiological and pathological processes in the context of the microtubules. Recent studies considered nuclear tau as a molecular marker of cell aging and aging-associated diseases, such as AD (8). Nuclear tau is reportedly indispensable for cellular responses against cellular injury and DNA damage (8, 55). Additionally, nuclear tau can organize and protect the chromatin during cellular aging (8, 56). The functional nucleolar tau is mostly dephosphorylated. Upon phosphorylation, tau dissociates from the DNA (55). The absence of functional tau due to mutation (such as P301L and P301S) might impair the genome-protective functions of tau and render the cells susceptible to chromosomal instability (55). REGγ deficiency or dysfunction also promotes genome instability (57). The present study demonstrated that the expression of tau is correlated with that of REGγ. REGγ depletion promoted the accumulation of phosphorylated tau in the nuclei, which suggested the correlation between REGγ-proteasome function and nuclear tau regulation. Future studies should focus on the roles of REGγ and nuclear tau in inducing genome instability during the pathogenesis of neurodegenerative diseases.

Previously, we had demonstrated that the accumulation of GSK3β contributes to the development of brain disorders in aged *REGγ* KO mice (47). GSK3β is an important kinase involved in the hyperphosphorylation of tau and the pathogenesis of aging-associated dementia (58, 59). Therefore, the loss of REGγ function may regulate the pathogenesis of neurodegenerative diseases at multiple levels. REGγ overexpression significantly mitigated the progression of neurodegenerative disorders (including AD-like cognitive impairments), loss of neurons and dendritic spines, formation of NFTs, and reduction of life span in mice.

Interestingly, REGγ was reported to play an important role in innate immune responses and inhibits the overactivation of immunoproteasome and consequential development of autoimmune diseases (60, 61). Our observation of microglial activation is evidenced by increased GFAP staining in the hippocampus and other brain regions in *REGγ* KO;PS19 in mice, suggesting a potential role of REGγ in the regulation of immune responses in neural system. Detailed molecular mechanisms by which REGγ deficiency enhance microglial activation need further analysis.

In summary, the findings of this study demonstrate that REGγ downregulation during aging or in age-related brain disorders is associated with predisposition to tauopathies and AD. REGγ-mediated proteasomal degradation of tau, especially phosphorylated tau, is a novel mechanism for the regulation of tau homeostasis. This may help to identify novel roles of nuclear tau in addition to its role as a microtubule-associated protein. Strategies to achieve REGγ gain of function may aid in the development of novel therapies for tau-related neurodegenerative diseases.

Experimental procedures

Generation of transgenic mice

All animal experiments were conducted according to the guidelines of the Institutional Animal Care and Use Committee of East China Normal University and human sample experiments were conducted according to the guidelines of the University Committee on Human Research Protection with the ethical approval number: HR 016-2021. The animal ethical committee approval number is m20200303. *REGγ* KO mice (C57BL/6J background) were generated as reported previously (47). Mice with cre transgenes (Camk2α-cre) and conditional *REGγ* alleles with the *R26-stop-FLAG* reporter (conditional

REGγ KI) were maintained under the same conditions described previously. Camk2α-cre mice and conditional *REGγ* KI mice were hybridized over 10 generations to obtain the stable genotype. *REGγ* OE;PS19 mice were originally from JAX Laboratory with Prnp-MAPT*P301S mutation on a mixed B6; C3-Tg background. PS19 mice were crossbred with *REGγ* KO, Camk2α-cre, and conditional *REGγ* KI mice over 10 generations to obtain the stable C57BL/6J background offspring Control;PS19, *REGγ* KO;PS19, and *REGγ* OE;PS19, respectively. Male C57BL/6J mice aged 3 to 24 months were used unless otherwise described. All animals were bred in the animal room under the following conditions: temperature, 20 to 25 °C; humidity, 40% to 70%; circadian cycle, 12 h light/dark cycle; food and water supply, *ad libitum*.

Bioinformatics analysis

The *PSME3* expression data were obtained from the GEO database. The GSE159699 dataset included the RNA-seq data of postmortem lateral temporal lobe of patients with AD (n = 12), aged healthy control (aged, n = 10), and young healthy control (young, n = 8). Gene expression was normalized to FPKM. *PSME3* expression in the old (n = 10) and AD (n = 12) datasets was comparatively analyzed. Additionally, the gene expression data GSE1297, which is a microarray data of hippocampal gene expression in healthy control and patients with AD exhibiting varying severity, were downloaded. *PSME3* expression in healthy control (n = 9) and severe AD (n = 7) cases were analyzed. RNA-seq and microarray data were separately analyzed using GEO query and Limma packages in R http://www.r-project.org/ as described (26).

Cell culture

HEK 293T (WT and *REGγ* knockout using TALENs), SH-SY5Y (shN-transfected and shR-transfected), and HT22 (control and si-REGγ-transfected) were used in this study (31, 47, 62). si-REGγ RNA sequences were shown in the Table S1. All cells originally obtained from ATCC were cultured in Dulbecco's modified Eagle's medium (DMEM) or DMEM/F-12 (1:1) supplemented with 15% fetal bovine serum (HyClone), 100 IU/ml penicillin, and 100 mg/ml streptomycin (Thermo Fisher Scientific) in a humidified incubator at 37 °C and 5% CO_2. Silencing RNA sequences were listed in the Table S3.

Western blotting

Hippocampus and auditory cortex were dissected and subjected to SDS-PAGE. The resolved proteins were transferred to a nitrocellulose membrane and the protein signals were detected using fluorescent secondary antibodies in the Image Studio system, following routine protocols. Antibodies were shown in the Table S2.

Immunostaining

Mice brain tissues were perfused with ice-cold PBS (1×) and 4% paraformaldehyde and fixed with 4% paraformaldehyde for 72 h at 4 °C. To terminate fixation, the brain tissues were incubated in a solution containing 4% acrylamide, 1 M glycine, and 0.1% Triton-X 100 in 1× PBS for 48 h at room temperature. The tissues were washed with 1× PBS and sectioned into 10 μm thick sections using a freezing microtome (Leica CM1950) in 1× PBS. The detailed staining process has been described elsewhere (47). The images were captured using Tissue Gnostics Tissue FAXS Plus ST (ZEISS) and THUNDER Image System (Leica) microscope.

Nissl, Golgi, and Gallyas–Braak staining

Nissl staining was performed using the kit from Beyotime Biotechnology (C0117), following the manufacturer's instructions. The sections adjacent to the stained area were selected to measure the size of the whole brain and the number of neurons using the software Unbiased Stereology Tissue FAX Plus ST (Tissue Gnostics). Golgi staining was performed with the FD rapid Golgi stain kit (FD Neuro Technologies, Inc), following a previously published protocol (63). Mice were perfused following routine protocols. The sections were also subjected to a modified Gallyas–Braak staining (64). The images were captured using Tissue Gnostics Tissue FAXS Plus ST and fluorescence microscope (Olympus DP74).

In vitro *degradation assay*

REGγ heptamers and 20S core proteins were purified as described previously (20). The target protein tau and tau (S396E) were translated using a translation kit with an appreciate reaction system (Promega), following the manufacturer's instructions. Degradation reaction conditions have been described elsewhere (20). The reaction mixture was incubated 30 °C for 3 h. All proteins were detected by Western blotting.

Plasmids

The pcDNA3.1-flag-REGγ and pcDNA3.1-GFP-REGγ constructs previously generated (34) were used in this study. Based on the *Homo sapiens* tau sequence, pcDNA3.1-Flag-tau, pcDNA3.1-GFP-tau, and PSG5-HA-tau constructs were generated. The mutant constructs PSG5-HA-tau (T231A), PSG5-HA-tau (T231E), PSG5-HA-tau (S396A), and PSG5-HA-tau (S396E) were generated based on the primary construct aforementioned. Primers were listed in Table S1 in the supplementary.

qRT-PCR

Total RNA was extracted from cells and mouse brain tissues using an RNA extraction reagent (Vazyme). The isolated RNA was reverse transcribed into complementary DNA (cDNA) using the Strand cDNA synthesis kit (Vazyme) in a 30 μl reaction mixture. The cDNA was subjected to qRT-PCR using ChamQ SYBR qPCR Master Mix (High ROX Premixed) (Vazyme) and Quant Studio 3.0 (Thermo Scientific). Each experiment was repeated in triplicates. The primer pairs used for quantitative PCR were listed as shown in Table S1 in the supplementary.

Immunoprecipitation

The transfection of 293T cells was performed as described previously. SH-SY5Y cells and the hippocampal tissues of PS19 mice were subjected to immunoprecipitation. Cells or tissues were collected and lysed as previously described (34). The flag-beads and protein A/G with antibodies were used to immune-precipitate the specific proteins. Immunoprecipitates were washed thrice with buffer. The samples were centrifuged and the pellets were suspended in protein loading buffer with SDS and subjected to Western blotting analysis. Antibodies used were listed as shown in Table S2 in the supplementary.

ChIP assay

ChIP assay was conducted according to a protocol from the Cold Spring Harbor Laboratory published online at http://cshprotocols.cshlp.org/. Primers and antibody used were listed as shown in Tables S1 and S2 in the supplementary.

Behavioral procedures

Open field test

Mouse activity in an open field was measured using the TruScan system (Coulbourn Instruments). Briefly, mice were placed in a 38 cm × 27 cm × 27 cm chamber with 50 lux illumination. The free locomotion of the mice for 15 min was tracked using Truscan 2.1. Locomotion was recorded every 5 min.

Morris water maze test

All experiments were performed in a pool (80 cm in diameter) filled with water at 24 to 26 °C to a depth of 1 to 2 cm over the platform. Mice aged 6 and 9 months were used for the experiment. For training, a submerged platform was placed in the center of a quadrant to enable the animal to determine the location of the platform, which was the only escape from the water. On day 6 (probe trial), the platform was removed, and each mouse was placed into the pool from one point. The route taken by the animal in the target quadrant was monitored for 30 s. All sessions (acquisition phase, probe trials, and reverse phase) were tracked using Ethovision XT14 software package (Noldus IT). Latency that monitors the time to locate the hidden platform under the water and platform crossing that indicates the number of times each mouse tries to swim over the removed platform was quantified. A cued platform was used to exclude the potential impact of motor dysfunction in PS19 mice.

Eight-arm radial maze

The eight-arm radial maze test enables the identification of mice that exhibit age-related AD progression (39). Before training, these mice had limited to no access to food to ensure that they were motivated to search for food in the maze during the test. The baits were restricted to the food cups. During the first 4 days of training, the food pellets (approximately 45 mg in weight) were placed in the food cups (each eight-arm terminal) and the central octagonal plate. The mice of the same group were allowed to search for food together for 10 min. On day 5 (test day), the pellets in all eight-arm terminal cups were placed in a single food cup. Every test was continued until all eight food pellets had been consumed or until 10 min had elapsed. The number of reference and working memory errors was determined.

NOR

To examine the recognition memory of mice, each mouse was allowed to move freely in an arena (27 cm length × 27 cm width × 27 cm height) for 3 days. During the first 3 days, the mice were allowed to adapt to the box for 10 min. On day 4, every mouse was allowed to freely explore the arena with two identical objects for 15 min and rest in the cage for 1 h after exploration. One of the objects was replaced with a new object with a similar material. The mouse was then allowed to freely explore the arena for 5 min. The time spent exploring the novel and familiar objects was recorded. The object was judged to be explored when the mouse touched the object with the nose, mouth, and front paw or when the nose, mouth, and front paw were at a distance of ≤2 cm from the object. The NOR index (NOI) was calculated as follows: NOI = new object exploration time/(new object exploration time + old object exploration time) × 100%. NOIs >50 and ≤50 indicate complete and incomplete new object recognition, respectively (65).

EPM test

Noncognitive deficits, such as anxiety and motivation are factors that may affect cognitive outcomes. The EPM apparatus comprised a gray poly vinyl chloride '+' maze with two open arms, two enclosed arms, and a central platform linking the arms. The apparatus was raised 40 cm above the floor. Each mouse was placed at the central platform facing an enclosed arm and allowed to freely explore for 5 min. Ethovision XT14 software package (Noldus IT) was used to record the progress of this experiment.

Statistical analysis

Quantitative data of independent samples were analyzed using GraphPad Prism 8.0 (GraphPad Software Inc) and represented as mean ± SEM. The means (including behavioral and image data) were compared using one-way ANOVA, two-way ANOVA, and two-tailed *t* test.

Data availability

All raw bioinformatics analysis data are available in the Gene Expression Omnibus repository under accession code GSE1297 and GSE159699. A version of the Alzheimer's disease (AD) genomics data can be visualized at http://www.alzdata.org/. And protein expression in brain can be visualized at https://mouse.brain-map.org/ and http://www.proteinatlas.org/. All original data are available on request. All the other data supporting the findings of this study are available in the article and Inventory of Supporting Information files. Source data are provided with this article.

Supporting information—This article contains supporting information (46, 47, 62).

Acknowledgments—We acknowledge Dr Bo Meng and Dongmin Yin for their helpful suggestions and the National Human Brian Bank for providing human brain tissue samples. Additionally, we thank the Zhongshan North Road Campus Animal Experimental Platform, ECNU.

Author contributions—X. L. and J. X. methodology; L. G., J. T., H. Z., and Y. L. formal analysis; J. T., H. Z., T. Y., S. K., and Y. L. investigation; L. G., T. Y., Y. Z., H. Z., and T. Y. resources; X. L., J. T., H. Z., R. E. M., and B. W. O. writing–original draft.

Funding and additional information—This work was supported by the National Natural Science Foundation of China (31730017) to X. L. and the NIH grant (3RO1HD008188-50S1) to B. W. O. The content is solely the responsibility of the authors and does not necessarily represent the official views of the National Institutes of Health.

Conflict of interest—The authors declare that they have no conflicts of interest with the contents of this article.

Abbreviations—The abbreviations used are: Aβ, amyloid-beta; AD, Alzheimer's disease; cDNA, complementary DNA; ChIP, chromatin immunoprecipitation; HA, hemagglutinin; KI, knock-in allele; NFTs, neuron fibrillary tangles; NOI, novel object index; NOR, novel object recognition; OA, okadaic acid; qRT-PCR, quantitative real-time PCR; UPS, ubiquitin-proteasome system.

References

1. Lee, V. M., Goedert, M., and Trojanowski, J. Q. (2001) Neurodegenerative tauopathies. *Annu. Rev. Neurosci.* **24**, 1121–1159
2. Alzheimer's Association. (2015) 2015 Alzheimer's disease facts and figures. *Alzheimers Dement.* **11**, 332–384
3. Yoshiyama, Y., Higuchi, M., Zhang, B., Huang, S. M., Iwata, N., Saido, T. C., *et al.* (2007) Synapse loss and microglial activation precede tangles in a P301S tauopathy mouse model. *Neuron* **53**, 337–351
4. Huang, Y. D., and Mucke, L. (2012) Alzheimer mechanisms and therapeutic strategies. *Cell* **148**, 1204–1222
5. Xu, Y., Du, S. Q., Marsh, J. A., Horie, K., Sato, C., Ballabio, A., *et al.* (2020) TFEB regulates lysosomal exocytosis of tau and its loss of function exacerbates tau pathology and spreading. *Mol. Psychiatry* **26**, 5925–5939
6. Hansson, O. (2021) Biomarkers for neurodegenerative diseases. *Nat. Med.* **27**, 954–963
7. Braak, H., and Braak, E. (1991) Neuropathological stageing of Alzheimer-related changes. *Acta Neuropathol.* **82**, 239–259
8. Bukar Maina, M., Al-Hilaly, Y. K., and Serpell, L. C. (2016) Nuclear tau and its potential role in Alzheimer's disease. *Biomolecules* **6**, 9
9. Gil, L., Nino, S. A., Capdeville, G., and Jimenez-Capdeville, M. E. (2021) Aging and Alzheimer's disease connection: nuclear Tau and Lamin A. *Neurosci. Lett.* **749**, 135741
10. Brier, M. R., Gordon, B., Friedrichsen, K., McCarthy, J., Stern, A., Christensen, J., *et al.* (2016) Tau and A beta imaging, CSF measures, and cognition in Alzheimer's disease. *Sci. Transl. Med.* **8**, 338ra366
11. Thijssen, E. H., La Joie, R., Strom, A., Fonseca, C., Iaccarino, L., Wolf, A., *et al.* (2021) Plasma phosphorylated tau 217 and phosphorylated tau 181 as biomarkers in Alzheimer's disease and frontotemporal lobar degeneration: a retrospective diagnostic performance study. *Lancet Neurol.* **20**, 739–752
12. Karran, E., and De Strooper, B. (2022) The amyloid hypothesis in Alzheimer disease: new insights from new therapeutics. *Nat. Rev. Drug Discov.* **21**, 306–318
13. Naseri, N. N., Wang, H., Guo, J., Sharma, M., and Luo, W. (2019) The complexity of tau in Alzheimer's disease. *Neurosci. Lett.* **705**, 183–194
14. Cline, H. (2003) Synaptic plasticity: importance of proteasome-mediated protein turnover. *Curr. Biol.* **13**, R514–R516
15. Speese, S. D., Trotta, N., Rodesch, C. K., Aravamudan, B., and Broadie, K. (2003) The ubiquitin proteasome system acutely regulates presynaptic protein turnover and synaptic efficacy. *Curr. Biol.* **13**, 899–910
16. Ye, J., Yin, Y., Liu, H., Fang, L., Tao, X., Wei, L., *et al.* (2020) Tau inhibits PKA by nuclear proteasome-dependent PKAR2alpha elevation with suppressed CREB/GluA1 phosphorylation. *Aging Cell* **19**, e13055
17. Keck, S., Nitsch, R., Grune, T., and Ullrich, O. (2003) Proteasome inhibition by paired helical filament-tau in brains of patients with Alzheimer's disease. *J. Neurochem.* **85**, 115–122
18. Myeku, N., and Duff, K. E. (2018) Targeting the 26S proteasome to protect against proteotoxic diseases. *Trends Mol. Med.* **24**, 18–29
19. Dubiel, W., Pratt, G., Ferrell, K., and Rechsteiner, M. (1992) Purification of an 11 S regulator of the multicatalytic protease. *J. Biol. Chem.* **267**, 22369–22377
20. Li, X., Amazit, L., Long, W., Lonard, D. M., Monaco, J. J., and O'Malley, B. W. (2007) Ubiquitin- and ATP-independent proteolytic turnover of p21 by the REGgamma-proteasome pathway. *Mol. Cell* **26**, 831–842
21. Yersak, J. M., Montie, H. L., Chevalier-Larsen, E. S., Liu, Y. H., Huang, L., Rechsteiner, M., *et al.* (2017) The 11S proteasomal activator REG gamma impacts polyglutamine-expanded androgen receptor aggregation and motor neuron viability through distinct mechanisms. *Front. Mol. Neurosci.* **10**, 159
22. Yu, G., Zhao, Y., He, J., Lonard, D. M., Mao, C. A., Wang, G., *et al.* (2010) Comparative analysis of REG{gamma} expression in mouse and human tissues. *J. Mol. Cell Biol.* **2**, 192–198
23. Ahadi, S., Zhou, W. Y., Rose, S. M. S. F., Sailani, M. R., Contrepois, K., Avina, M., *et al.* (2020) Personal aging markers and ageotypes revealed by deep longitudinal profiling. *Nat. Med.* **26**, 83–90
24. Johnson, E. C. B., Dammer, E. B., Duong, D. M., Ping, L., Zhou, M., Yin, L., *et al.* (2020) Large-scale proteomic analysis of Alzheimer's disease brain and cerebrospinal fluid reveals early changes in energy metabolism associated with microglia and astrocyte activation. *Nat. Med.* **26**, 769–780
25. Blalock, E. M., Geddes, J. W., Chen, K. C., Porter, N. M., Markesbery, W. R., and Landfield, P. W. (2004) Incipient Alzheimer's disease: microarray correlation analyses reveal major transcriptional and tumor suppressor responses. *Proc. Natl. Acad. Sci. U. S. A.* **101**, 2173–2178
26. Nativio, R., Lan, Y., Donahue, G., Sidoli, S., Berson, A., Srinivasan, A. R., *et al.* (2020) An integrated multi-omics approach identifies epigenetic alterations associated with Alzheimer's disease. *Nat. Genet.* **52**, 1024–1035
27. Satoh, J., Yamamoto, Y., Asahina, N., Kitano, S., and Kino, Y. (2014) RNA-seq data mining: downregulation of NeuroD6 serves as a possible biomarker for Alzheimer's disease brains. *Dis. Markers* **2014**, 123165
28. Li, L., Zhao, D., Wei, H., Yao, L., Dang, Y., Amjad, A., *et al.* (2013) REGgamma deficiency promotes premature aging via the casein kinase 1 pathway. *Proc. Natl. Acad. Sci. U. S. A.* **110**, 11005–11010
29. He, J., Cui, L., Zeng, Y., Wang, G., Zhou, P., Yang, Y., *et al.* (2012) REGgamma is associated with multiple oncogenic pathways in human cancers. *BMC Cancer* **12**, 75
30. Wang, Z. H., Wu, W., Kang, S. S., Liu, X., Wu, Z., Peng, J., *et al.* (2018) BDNF inhibits neurodegenerative disease-associated asparaginyl endopeptidase activity via phosphorylation by AKT. *JCI Insight* **3**, e99007
31. Liu, J., Yu, G., Zhao, Y., Zhao, D., Wang, Y., Wang, L., *et al.* (2010) REGgamma modulates p53 activity by regulating its cellular localization. *J. Cell Sci.* **123**, 4076–4084
32. Shafiei, S. S., Guerrero-Munoz, M. J., and Castillo-Carranza, D. L. (2017) Tau oligomers: cytotoxicity, propagation, and mitochondrial damage. *Front. Aging Neurosci.* **9**, 83
33. Fernandez, J. J., Candenas, M. L., Souto, M. L., Trujillo, M. M., and Norte, M. (2002) Okadaic acid, useful tool for studying cellular processes. *Curr. Med. Chem.* **9**, 229–262
34. Gao, X., Wang, Q., Wang, Y., Liu, J., Liu, S., Liu, J., *et al.* (2020) The REGgamma inhibitor NIP30 increases sensitivity to chemotherapy in p53-deficient tumor cells. *Nat. Commun.* **11**, 3904

35. Dong, S., Jia, C., Zhang, S., Fan, G., Li, Y., Shan, P., *et al.* (2013) The REGgamma proteasome regulates hepatic lipid metabolism through inhibition of autophagy. *Cell Metab.* **18**, 380–391
36. Arriagada, P. V., Growdon, J. H., Hedley-Whyte, E. T., and Hyman, B. T. (1992) Neurofibrillary tangles but not senile plaques parallel duration and severity of Alzheimer's disease. *Neurology* **42**, 631–639
37. Togo, T., and Dickson, D. W. (2002) Tau accumulation in astrocytes in progressive supranuclear palsy is a degenerative rather than a reactive process. *Acta Neuropathol.* **104**, 398–402
38. Martin, E., Amar, M., Dalle, C., Youssef, I., Boucher, C., Le Duigou, C., *et al.* (2019) New role of P2X7 receptor in an Alzheimer's disease mouse model. *Mol. Psychiatry* **24**, 108–125
39. Stevens, L. M., and Brown, R. E. (2015) Reference and working memory deficits in the 3xTg-AD mouse between 2 and 15-months of age: a cross-sectional study. *Behav. Brain Res.* **278**, 496–505
40. Watt, G., Przybyla, M., Zak, V., van Eersel, J., Ittner, A., Ittner, L. M., *et al.* (2020) Novel behavioural characteristics of male human P301S mutant tau transgenic mice - a model for tauopathy. *Neuroscience* **431**, 166–175
41. Wang, H., Liu, X., Chen, S., and Ye, K. (2018) Spatiotemporal activation of the C/EBPbeta/delta-secretase axis regulates the pathogenesis of Alzheimer's disease. *Proc. Natl. Acad. Sci. U. S. A.* **115**, E12427–E12434
42. Xia, Y., Wang, Z. H., Zhang, J., Liu, X., Yu, S. P., Ye, K. X., *et al.* (2020) C/EBPbeta is a key transcription factor for APOE and preferentially mediates ApoE4 expression in Alzheimer's disease. *Mol. Psychiatry* **26**, 6002–6022
43. Wang, Z. H., Gong, K., Liu, X., Zhang, Z., Sun, X., Wei, Z. Z., *et al.* (2018) C/EBPbeta regulates delta-secretase expression and mediates pathogenesis in mouse models of Alzheimer's disease. *Nat. Commun.* **9**, 1784
44. Wang, Z. H., Xia, Y., Liu, P., Liu, X., Edgington-Mitchell, L., Lei, K., *et al.* (2021) ApoE4 activates C/EBPbeta/delta-secretase with 27-hydroxycholesterol, driving the pathogenesis of Alzheimer's disease. *Prog. Neurobiol.* **202**, 102032
45. Takayama, K., Kawabata, K., Nagamoto, Y., Inamura, M., Ohashi, K., Okuno, H., *et al.* (2014) CCAAT/enhancer binding protein-mediated regulation of TGFbeta receptor 2 expression determines the hepatoblast fate decision. *Development* **141**, 91–100
46. Ali, A., Wang, Z., Fu, J., Ji, L., Liu, J., Li, L., *et al.* (2013) Differential regulation of the REGgamma-proteasome pathway by p53/TGF-beta signalling and mutant p53 in cancer cells. *Nat. Commun.* **4**, 2667
47. Lv, Y., Meng, B., Dong, H., Jing, T., Wu, N., Yang, Y., *et al.* (2016) Upregulation of GSK3beta contributes to brain disorders in elderly REGgamma-knockout mice. *Neuropsychopharmacology* **41**, 1340–1349
48. Jiang, S., and Bhaskar, K. (2020) Degradation and transmission of tau by autophagic-endolysosomal networks and potential therapeutic targets for tauopathy. *Front. Mol. Neurosci.* **13**, 586731
49. Lee, M. J., Lee, J. H., and Rubinsztein, D. C. (2013) Tau degradation: the ubiquitin-proteasome system versus the autophagy-lysosome system. *Prog. Neurobiol.* **105**, 49–59
50. Wang, Y., Martinez-Vicente, M., Kruger, U., Kaushik, S., Wong, E., Mandelkow, E. M., *et al.* (2009) Tau fragmentation, aggregation and clearance: the dual role of lysosomal processing. *Hum. Mol. Genet.* **18**, 4153–4170
51. Caballero, B., Wang, Y., Diaz, A., Tasset, I., Juste, Y. R., Stiller, B., *et al.* (2018) Interplay of pathogenic forms of human tau with different autophagic pathways. *Aging Cell* **17**, e12692
52. Kruger, U., Wang, Y., Kumar, S., and Mandelkow, E. M. (2012) Autophagic degradation of tau in primary neurons and its enhancement by trehalose. *Neurobiol. Aging* **33**, 2291–2305
53. Luo, H. B., Xia, Y. Y., Shu, X. J., Liu, Z. C., Feng, Y., Liu, X. H., *et al.* (2014) SUMOylation at K340 inhibits tau degradation through deregulating its phosphorylation and ubiquitination. *Proc. Natl. Acad. Sci. U. S. A.* **111**, 16586–16591
54. Reddy, P. H., and Oliver, D. M. (2019) Amyloid beta and phosphorylated tau-induced defective autophagy and mitophagy in Alzheimer's disease. *Cells* **8**, 488
55. Sultan, A., Nesslany, F., Violet, M., Begard, S., Loyens, A., Talahari, S., *et al.* (2011) Nuclear tau, a key player in neuronal DNA protection. *J. Biol. Chem.* **286**, 4566–4575
56. Gil, L., Federico, C., Pinedo, F., Bruno, F., Rebolledo, A. B., Montoya, J. J., *et al.* (2017) Aging dependent effect of nuclear tau. *Brain Res.* **1677**, 129–137
57. Zannini, L., Lecis, D., Buscemi, G., Carlessi, L., Gasparini, P., Fontanella, E., *et al.* (2008) REGgamma proteasome activator is involved in the maintenance of chromosomal stability. *Cell Cycle* **7**, 504–512
58. Schaffer, B. A., Bertram, L., Miller, B. L., Mullin, K., Weintraub, S., Johnson, N., *et al.* (2008) Association of GSK3B with Alzheimer disease and frontotemporal dementia. *Arch. Neurol.* **65**, 1368–1374
59. Lee, S. J., Chung, Y. H., Joo, K. M., Lim, H. C., Jeon, G. S., Kim, D., *et al.* (2006) Age-related changes in glycogen synthase kinase 3beta (GSK3beta) immunoreactivity in the central nervous system of rats. *Neurosci. Lett.* **409**, 134–139
60. Yao, L., Zhou, L., Xuan, Y., Zhang, P., Wang, X., Wang, T., *et al.* (2019) The proteasome activator REGgamma counteracts immunoproteasome expression and autoimmunity. *J. Autoimmun.* **103**, 102282
61. Zhou, L., Yao, L., Zhang, Q., Xie, W., Wang, X., Zhang, H., *et al.* (2020) REGgamma controls Th17 cell differentiation and autoimmune inflammation by regulating dendritic cells. *Cell. Mol. Immunol.* **17**, 1136–1147
62. Zhu, X., Yang, M., Lin, Z., Mael, S. K., Li, Y., Zhang, L., *et al.* (2022) REGgamma drives Lgr5(+) stem cells to potentiate radiation induced intestinal regeneration. *Sci. China Life Sci.* **65**, 1608–1623
63. Glaser, E. M., and Van der Loos, H. (1981) Analysis of thick brain sections by obverse-reverse computer microscopy: application of a new, high clarity Golgi-Nissl stain. *J. Neurosci. Methods* **4**, 117–125
64. Uchihara, T., Kondo, H., Kosaka, K., and Tsukagoshi, H. (1992) Selective loss of nigral neurons in Alzheimer's disease: a morphometric study. *Acta Neuropathol.* **83**, 271–276
65. Zlomuzica, A., Tress, O., Binder, S., Rovira, C., Willecke, K., and Dere, E. (2012) Changes in object recognition and anxiety-like behaviour in mice expressing a Cx47 mutation that causes Pelizaeus-Merzbacher-like disease. *Dev. Neurosci.* **34**, 277–287